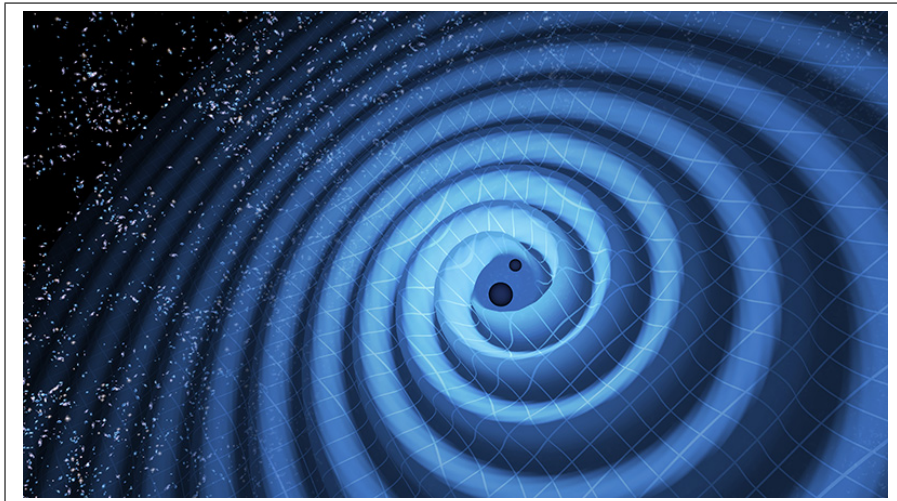**Universiteit Utrecht**

Opleiding Natuur- en Sterrenkunde

Probing the existence of Primordial Black Holes with Gravitational Waves

BACHELOR THESIS

Joren Ziel

Supervisor:

Dr. Sarah CAUDILL

Institute for Gravitational and Subatomic Physics

June 16, 2021

Abstract

In recent years gravitational waves have attracted a lot of attention because they are a novel way of studying the properties and mergers of black holes and neutron stars. Now, we use them to probe the existence of a different type of black holes; primordial black holes (PBHs). First, we use the thermal history of the early Universe to infer the PBH mass spectrum. We find that it has peaks at 5×10^{-4}, 2, 100 and $6 \times 10^6 M_\odot$. From this, we see that PBHs could comprise all of the cold dark matter in the Universe. We then take into account the sensitivity of the LIGO and Virgo detectors during the O2 run and we find that we can detect black hole mergers with masses around 2 and $100 M_\odot$, opening up the possibility of probing the existence of PBHs in the near future.

Front page: The picture shows a compact binary black hole system that emits gravitational waves. It is taken from:

`https://physicsworld.com/a/ligo-detects-second-black-hole-merger/`.

Contents

1 Introduction

When Einstein published his theory of General Relativity (GR) in 1915, it completely changed our understanding of gravity. It was no longer seen as a force, but as a geometric property of the fabric of the Universe; space-time. Space-time can be curved by the mass and energy of objects and this curvature tells other objects how to move. Not only does it change the way we look at gravity, but it also has some rather interesting consequences. Two of the most important implications are the existence of black holes (BHs), regions in space-time that are so distorted by mass and energy, that not even light can escape from them, and the existence of gravitational waves (GWs); ripples in space-time, propagating as waves at the speed of light. Both BHs and GWs have been the subject of many researches done in the last century and this thesis is no exception. By doing some calculations on gravitational waves, Einstein noted that they were very weak and would probably never be observed. Nevertheless, nearly one hundred years later, the laser interferometers LIGO and Virgo detected the first gravitational waves in 2016 and have detected dozens more since then. Now, in this thesis we want to probe the existence of a primordial black hole (PBH) population and verify whether or not we can detect them with the current LIGO/Virgo interferometers. PBHs are black holes formed very early on in the Universe and are as of now, only hypothetical. By looking at the thermal history of the early Universe, we infer what the mass spectrum of such a PBH population would look like. Then, we take into account the sensitivity of the interferometers during the second observing run (O2) and predict the possibility of detecting (parts of) a PBH population. This is mostly a re-evaluation of the research done by Carr *et al.* [3]. However, we made and used a Python notebook for our figures and calculations, instead of a Mathematica notebook. We find that changes in the relativistic degrees of freedom cause increased probabilities of PBH formation, which results in peaks in the PBH mass spectrum whenever this happens. Most notably, you have the main peak at PBH masses (M) of $M \approx 2M_\odot$, and other smaller peaks at $M \approx 100M_\odot$, $M \approx 5 \times 10^{-4} M_\odot$ and at $M \approx 6 \times 10^6 M_\odot$. All of these peaks lie in regions where you would not expect stellar black holes from the current astrophysical models, making it easier to distinguish their primordial origin. From looking at the O2 sensitivity of LIGO/Virgo, we also find that we can actually detect mergers of PBHs with both masses around $2M_\odot$ or with both masses

around $100 M_\odot$, the latter being the most probable of the two. The remainder of this thesis is organized as follows. In Chapter 2 we look at gravitational waves; how they are derived from GR, how they are detected and what their sources are. In Chapter 3 we look at black holes; what they are, what classes you have and how they can form binary systems. Chapter 4 is going to look at primordial black holes in more detail; when they are formed, what their mass spectrum looks like and how often they merge. In Chapter 5 we give our results and in Chapter 6 we conclude and discuss our findings. Finally, we have an Appendix (A) where we look at the differences in interpolating between Mathematica and Python.

2 Gravitational waves

2.1 Linearized Gravity

Gravitational waves were predicted to exist by Einstein in his theory of General Relativity as disturbances in the curvature of space-time caused by accelerated masses. These disturbances propagate as waves from their source at the speed of light and they transport energy in the form of gravitational radiation. In GR, Einstein derived what is now known as the Einstein field equations [14]:

$$G_{\mu\nu} = \frac{8\pi G}{c^4} T_{\mu\nu}, \tag{1}$$

where the Einstein tensor $G_{\mu\nu}$ is constructed from the metric $g_{\mu\nu}$ and its derivatives with respect to the coordinates, G is the gravitational constant, c is the speed of light and $T_{\mu\nu}$ is the energy momentum tensor. To get a bit of understanding into the nature of GWs, we study them where the gravitational fields are weak. In this case, we can write the metric as

$$g_{\mu\nu} = \eta_{\mu\nu} + h_{\mu\nu}, \tag{2}$$

where $\eta_{\mu\nu}$ is the Minkowski metric of special relativity $diag(-1, 1, 1, 1)$ and $h_{\mu\nu}$ is a small correction due to the weak gravitational fields ($|h_{\mu\nu}| \ll 1$). The next step is to 'linearize' the Einstein field equations by substituting Eq. 2 into Eq. 1 and only keeping terms that are linear

in $h_{\mu\nu}$ and its derivatives. To simplify notation in the process, we define a new tensor

$$\bar{h}_{\mu\nu} = h_{\mu\nu} - \frac{1}{2}\eta_{\mu\nu}h, \tag{3}$$

where $h = \eta^{\mu\nu}h_{\mu\nu}$. This then gives for the linearized Einstein field equations

$$\Box\bar{h}_{\mu\nu} + \eta_{\mu\nu}\partial^\rho\partial^\sigma\bar{h}_{\rho\sigma} - \partial^\rho\partial_\nu\bar{h}_{\mu\rho} - \partial^\rho\partial_\mu\bar{h}_{\nu\rho} = -\frac{16\pi G}{c^4}T_{\mu\nu}, \tag{4}$$

where $\partial^\rho = \eta^{\rho\alpha}\partial_\alpha$, and

$$\Box \equiv \partial_\mu\partial^\mu$$
$$= \eta^{\mu\nu}\partial_\mu\partial_\nu \tag{5}$$
$$= -\frac{\partial^2}{c^2\partial t^2} + \frac{\partial^2}{\partial x^2} + \frac{\partial^2}{\partial y^2} + \frac{\partial^2}{\partial z^2}$$

is the d'Alembertian. Eq. 4 is gauge invariant, which allows us to do a gauge transformation using the harmonic gauge ($\partial_\mu\bar{h}_{\mu\nu} = 0$). This transformation reduces Eq. 4 to the rather simple equation

$$\Box\bar{h}_{\mu\nu} = -\frac{16\pi G}{c^4}T_{\mu\nu}. \tag{6}$$

Now, outside the source, $T_{\mu\nu} = 0$. So, Eq. 6 becomes a wave equation

$$\Box\bar{h}_{\mu\nu} = \left(-\frac{\partial^2}{c^2\partial t^2} + \frac{\partial^2}{\partial x^2} + \frac{\partial^2}{\partial y^2} + \frac{\partial^2}{\partial z^2}\right)\bar{h}_{\mu\nu} = 0, \tag{7}$$

and we can see that gravitational waves follow naturally from linearized gravity.

2.2 Gravitational wave detectors

Since GWs are disturbances in the curvature of space-time, they periodically stretch and compress space in directions perpendicular to the propagation direction. However, as Einstein already noted, these effects are very hard if not impossible to detect, since the relative changes are very small:

$$\frac{\Delta L}{L} \lesssim 10^{-22}, \tag{8}$$

where ΔL is the difference in the arm length and L is the arm length. Nevertheless, there are detectors capable of detecting these changes; kilometers long laser interferometers. The basic idea of a laser interferometer can be seen in Fig. 1; A laser beam is being shone onto the beam splitting mirror, which causes half of the laser light to go down one detector arm and the other half down another detector arm perpendicular to the first one. At the end of each arm, there is a mirror that reflects the laser light back through the arm and onto the detector. The interferometer is set up in such a way, that if there is no GW going through it, the two laser beams cancel each other out by destructive interference and no signal can be seen at the detector. If there is a GW travelling through the detector however, then periodically one arm is stretched and the other compressed, causing the laser beams to change their relative phase which in turn ruins the destructive interference. This leads to a laser signal being able to reach the detector, and thus a measurement of a gravitational wave. There are currently five
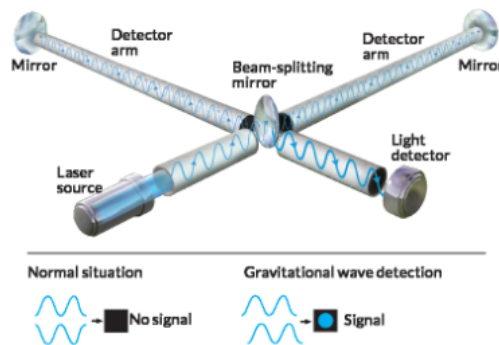

Figure 1: The principle of a laser interferometric gravitational wave detector from Ref. [14].

gravitational wave detectors: two Advanced LIGO interferometers in the US (one in Washington state and the other in Louisiana, both having 4 km arms), Advanced Virgo in Italy (with 3 km arms), KAGRA in Japan (also 3 km arms), and GEO600 in Germany (600 m arms), with more to come in the near future (LIGO-India, Einstein telescope and LISA).

2.3 Gravitational wave sources

Now that we know how the existence of gravitational waves was derived from linearized gravity and how we can detect them, we look at sources of gravitational waves. There are multiple

different types of sources and we will discuss them shortly here.

2.3.1 Compact binary coalescence

The first one and most detected/studied one is the so called compact binary coalescence (CBC). Here, the GWs are emitted from two closely orbiting neutron stars (NS), black holes or a combination of a neutron star and black hole. To begin with, the two objects are in a wide, typically elliptic orbit around their common center of gravity. Since these objects are massive and extremely dense, they cause a huge curvature of space-time, and will emit GWs in their orbit. These GWs carry energy and angular momentum and thus, the orbits shrink and become more circular. When the objects are close enough together that their GWs can be detected, their orbits are assumed to be circularized and we have the so called quasi-circular *inspiral*. This goes on until the innermost stable circular orbit (ISCO) is reached, and after this the objects *plunge* towards each other and *merge* into a single, highly excited black hole or a massive, very asymmetric neutron star. This final object will then undergo *ringdown*, during which the excitations are shedded until it settles into a dormant state. A schematic overview of the CBC process with the produced gravitational wave can be seen in Fig. 2.
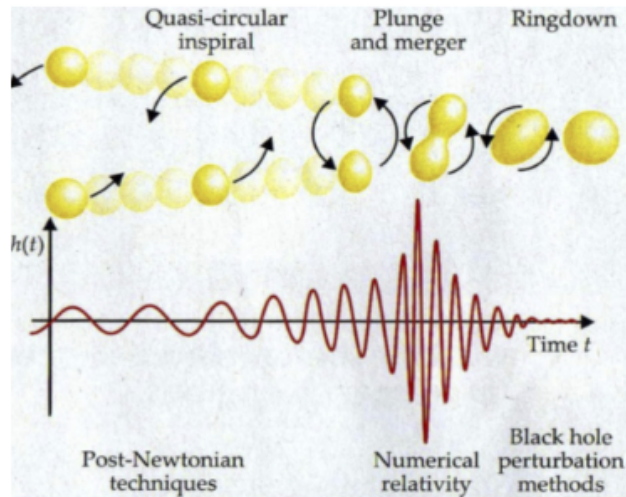

Figure 2: Schematic overview of the CBC process for two black holes (top) and the gravitational wave signal that is produced (bottom) from Ref. [14].

2.3.2 Continuous

The second source of GWs are systems with a fairly constant and well-defined frequency. Examples of such systems are binary systems far from merger and fast rotating single bodies with a large mountain or other irregularity on it. The GWs from these systems are weaker than from CBC events and are rather continuous in time, hence the name continuous gravitational waves. Important candidates for such GWs are neutron stars in our own Galaxy. However, current detectors are not sensitive enough to detect them yet. Important to keep in mind as well is that these systems do lose energy over time, since they emit GWs and possibly electromagnetic waves, and so will eventually have different gravitational wave signals. This effect is very small however, so these systems are for the most part constant, especially compared to CBC events, which change rapidly in time.

2.3.3 Bursts

A burst gravitational wave event is an event where a large amount of gravitational energy is released over a very short period of time (less than a few seconds). The events that could produce these GWs are for example supernovae or gamma ray bursts [8], but there is too little known about the details of these events and it is therefore hard to anticipate the exact wave forms.

2.3.4 Stochastic

Stochastic gravitational waves are relics of the early evolution of the Universe. They are a combination of many random, independent GW events, which result in an all-sky GW background, very similar to the cosmic microwave background (CMB). Since these GWs are produced very early on in the Universe, they are stretched due to the expansion of the Universe and are therefore very weak and hard to detect with ground-based interferometers.

3 Binary black holes

3.1 What is a black hole?

In this chapter we are going to describe in details the nature of BHs. Just like GWs, BHs were a prediction from Einsteins theory of general relativity. If you solve Einsteins field equations (Eq. 1) for the gravitational field outside a static spherically symmetric mass M, with zero electric charge and angular momentum, you get the Schwarzschild metric [6]

$$ds^2 = -\left(1 - \frac{2GM}{rc^2}\right)c^2dt^2 + \left(1 - \frac{2GM}{rc^2}\right)^{-1}dr^2 + r^2d\theta^2 + r^2\sin^2\theta d\phi^2, \tag{9}$$

where r is the distance to the mass. As can be seen from Eq. 9, there is a singularity at the so called Schwarzschild radius

$$R_s = \frac{2GM}{c^2}. \tag{10}$$

If the mass M is compressed within this radius, no signal can escape from within R_s, not even light. For most objects this radius is far smaller than its actual radius, but for some stars this radius is achieved at the end of their life (see section 3.2.1). There are also black hole solutions for more general scenarios, which include spin and electric charge. In general, the no-hair theorem states that black holes can be completely characterized by three parameters: mass, angular momentum and electric charge. This means that information about the matter composition that formed the BH is lost, to the frustration of many physicists. Since no light can escape from the black hole, it has very few (known) physical features. One of the features it does have, is the event horizon. This horizon is the boundary beyond which no events (signals) can affect an observer outside of it. This horizon is also used as the size of the black hole and for non-spinning neutral black holes it is exactly the Schwarzschild radius (see Eq. 10). For black holes with non-zero spin and/or electric charge however, it is smaller than the Schwarzschild radius. Another feature of a black hole is the (gravitational) singularity at the center. This singularity holds all of the mass of the black hole in a region of zero volume, which means that it has an infinite density and infinite space-time curvature. Another consequence of light not being able to escape from a black hole is that it is (almost) impossible to directly observe

them. There are however multiple ways of indirectly observing them. The first one is due to its gravitational effect on nearby celestial bodies; if a star is close enough to a black hole, the stars orbit is affected by it, which can be seen by astronomers. From this orbit they can infer the mass and position of a black hole. Another way to detect them is by a process called gravitational lensing. In this process, light emitted from a distant source is bent by some mass (which could be a BH) as it travels through the Universe. In the extreme cases, which is if it travels very closely to the mass or if the mass is enormous, the light gets so distorted that the original source can be seen as a ring or as multiple sources. In the non-extreme cases, the lensing can be detected by analyzing many different sources and looking for small distortions. From this lensing, we can infer the position and mass of a black hole. A third way of detecting black holes is by CBC processes which are detected by GWs. From the waveform of the GW, we can calculate the mass of the system and if it is detected by multiple different detectors, the position of the CBC can be approximated. The final way of detecting black holes is by their accretion disk. If there is matter around a black hole, it can orbit the black hole and be pulled into it by the gravity of the BH. During this process the matter can reach velocities close to the speed of light and there is a lot of friction. This causes the matter to heat up to very high temperatures and leads to emission of electromagnetic radiation, mainly in the x-ray range. This radiation can then be detected and from this the position of the black hole can be obtained.

3.2   Black holes classes

In this thesis, we focus on two possible classes of black holes.

3.2.1   Astrophysical

The first class of black holes we will consider are those formed from normal stellar evolution pathways. We will denote these as astrophysical black holes. These black holes are formed from very massive stars ($m \gtrsim 20 \ M_\odot$ [10]). When these heavy stars reach the end of their lives, the radiation pressure generated by the nucleosynthesis in its core is no longer enough to withstand the gravitational collapse under its own weight. What happens next depends on the mass and composition of the star. If the star has a very large mass ($m \gtrsim 40 \ M_\odot$) and

is very compact, which is mostly the case for metal-poor stars, it will collapse directly into a black hole. Since (almost) no mass is ejected during the formation, these black holes are quite massive. Another thing happens for less massive stars (or stars with more metals); when the core of the star collapses, the outer layers are ejected at high speeds, which causes a supernova explosion. During the supernova, the majority of the stars mass is lost, which leads to the formation of either a lighter black hole or a neutron star from the star's core. The masses of the astrophysical black holes range from $5 - 50M_\odot$ [1]. Black holes with a mass above $50M_\odot$ are not formed due to a process called pair instability [1]. This process happens in stars with a helium core with $M \geq 60M_\odot$. In these stars the central temperature reaches $\sim 10^9 \ K$, which causes the efficient production of electron-positron pairs. This in turn leads to a reduction of the radiation pressure, which causes the star to partially collapse under its gravity. This then causes the temperature to further increase, which causes thermonuclear reactions that result in an explosion, leaving no stellar remnant behind. Since normal stellar evolution pathways can not form black holes with certain masses, you have so called gaps in the astrophysical BH mass range. The region of black hole masses $\geq 50 \ M_\odot$ is called the upper mass gap. There is also a lower mass gap between the heaviest neutron stars and the lightest astrophysical black holes, ranging from $\sim 2.5 \ M_\odot$ to $5 \ M_\odot$ [1].

3.2.2 Primordial

The other class of black holes are the primordial ones. These primordial black holes are hypothetical and are expected to have formed early on in the Universe (in the radiation dominated epoch). Because they don't form from stars, their mass range is far bigger than that of astrophysical ones. Since these black holes are the main focus of this thesis, their properties are explained in more detail in the chapter 4.

3.3 Binary formation

In order for a CBC event to be detected, there must first form a binary black hole (BBH) system. The most straightforward way is from a binary system of two massive stars (MS). In this system the most massive star will collapse into a black hole first. If the objects do not orbit too close to each other and the companion is not disrupted by for example a supernova

during the black hole formation, the system will remain stable. When the second star reaches the later stages of its evolution, it will expand. This causes the outer layers of the giant star to reach the black hole and the system develops what is known as a common envelope. Since the black hole and the core of the companion star orbit each other inside this common envelope, they experience drag and lose kinetic energy. This kinetic energy is transferred to the envelope as thermal energy and if it is sufficient, it will cause the envelope to be ejected leaving behind a stable binary of a black hole and the core of the companion star. This core can then collapse to a black hole and you have a binary black hole system. If the thermal energy is not enough to eject the envelope however, the binary system will continue to lose kinetic energy due to the drag and you get a premature merger of the BH and the core. An illustration of this process can be seen on the left-hand side of Fig. 3. Another way to form binary black hole systems is from over-contact binary evolution [11]. When two massive stars are in a tight binary and are fast rotators, they remain fully mixed due to their tidally induced high spins. This prevents the binary to merge prematurely resulting in a possible BBH system. A completely different way to form BBH systems occurs in star clusters. If you have a binary system there with one black hole and a companion star, the system can interact with a single stellar object, which replaces the companion star. This process is called dynamical exchange. If the stellar object is a black hole, a binary black hole system can be formed. This resulting BBH system can be more tightly bound if another stellar object interacts with the system, without replacing one of the constituents. This is called hardening and speeds up the merger of the BBH system. A cartoon of this process can be seen in Fig. 3 on the right-hand side.
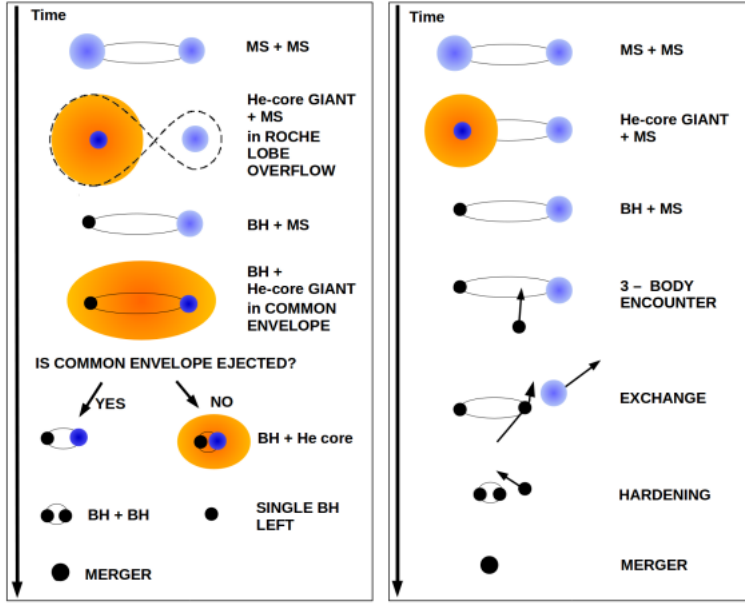
Figure 3: Illustration of BBH formation from common envelope on the left-hand side and from dynamical exchange on the right-hand side. Image taken from Ref. [10]

4 Primordial black holes

4.1 Thermal History

To understand how and when PBHs form, we need to look at the thermal history of the Universe. Since the number of relativistic degrees of freedom (g_*) is determined by how many Standard Model (SM) particles are relativistic, it depends on the temperature and we can therefore use it to look at the thermal history. A formula for calculating it is given by [13]:

$$g_*(T) = \sum_B g_B \left(\frac{T_B}{T}\right)^4 + \frac{7}{8} \sum_F g_F \left(\frac{T_F}{T}\right)^4, \tag{11}$$

where T is the photon temperature and T_B the temperature for each boson and T_F the temperature for each fermion. The degrees of freedom for individual particles is determined by their spin degrees of freedom, possible colour charges and for vector bosons also by whether or not they have a mass. Changes in g_* induce changes in the equation-of-state parameter (w). This w is used to express the equation-of-state of a fluid and is related to the pressure p and energy density ρ of the fluid by $w = p/\rho$ [6]. From Ref. [9], we get that $p \propto g_*$. This

11

means that w reduces whenever g_* suddenly reduces, which can be seen in figure 4. After each drop however, it goes back to its relativistic value of 1/3. At $T \approx 200\ GeV$, all SM particles are relativistic and this gives $g_* = 106.75$. The first particle to become non-relativistic is the top quark at $T \approx 172\ GeV$. This causes g_* to lower a bit. The next drop in g_* occurs not much later, at around $T \approx 80\ GeV$, when the W and Z boson become non-relativistic. After this, $g_* = 86.75$ for some time. The next significant and also the largest drop in g_* occurs at around $T \approx 200\ MeV$, when the quantum chromodynamic (QCD) phase transition happens and free quarks condense into protons and neutrons. This gives $g_* = 17.25$. Not long after this, the pions and muons become non-relativistic and you have $g_* = 10.75$. After this, g_* remains constant until $T \approx 1\ MeV$ when it drops to $g_* = 3.36$ due to e^+e^- annihilation and neutrino decoupling. During these changes in g_* and resulting dips in w, the probability of gravitational collapse is modified and PBHs are more likely to form.
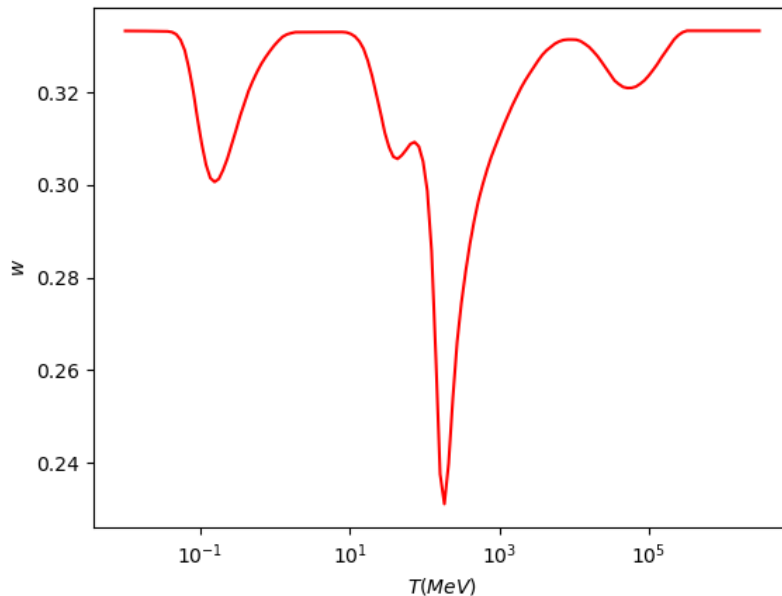

Figure 4: The equation-of-state parameter w as a function of the temperature T in MeV.

4.2 PBH formation

This subsection follows the discussion from Ref. [3] closely. There are a lot of different ways a PBH could form [4]. However, for all of them there must be some overdensity δ in some region of the early Universe. If this overdensity is bigger than some threshold value δ_c, which depends on

the equation of state and density profile, it will collapse into a PBH when it reenters the Hubble horizon. Since δ_c is a function of w, the thermal history of the Universe is quite important for understanding the mass function of PBHs. If the PBHs form from Gaussian inhomogeneities with a root-mean-square amplitude δ_{rms}, the fraction of horizon patches undergoing collapse to PBHs when the temperature of the Universe is T is given by [5]

$$\beta(M) \approx \text{erfc}\left[\frac{\delta_c(w[T(M)])}{\sqrt{2}\delta_{rms}(M)}\right], \tag{12}$$

where 'erfc' is the complementary error function and the temperature is related to the mass of the PBH by

$$T \approx 200\sqrt{M_\odot/M} \ MeV. \tag{13}$$

From this, it follows that $\beta(M)$ is exponentially sensitive to the equation-of-state parameter. The present fraction of cold dark matter (CDM) in PBHs with a mass around M is given by

$$f_{PBH} \approx 2.4\beta(M)\sqrt{\frac{M_{eq}}{M}}, \tag{14}$$

where $M_{eq} = 2.8 \times 10^{17}M_\odot$ is the horizon mass at matter-radiation equality. The numerical factor is calculated from $2(1 + \Omega_b/\Omega_{CDM})$, with $\Omega_b = 0.0456$ and $\Omega_{CDM} = 0.245$ being the baryon and CDM density parameters [2]. For δ_{rms}, we assume a spectrum of the form

$$\delta_{rms} = A\left(\frac{M}{M_\odot}\right)^{(1-n_s)/4}, \tag{15}$$

where A is the spectral amplitude and n_s the spectral index. Using these four equations gives us the mass spectra as shown in figure 5. The spectra all show the most dominant peak at $M \approx 2M_\odot$ and other smaller peaks at $5 \times 10^{-4}M_\odot$, $10^2 M_\odot$ and $6 \times 10^6 M_\odot$, corresponding to the changes in the number of relativistic degrees of freedom as predicted from the thermal history of the Universe.
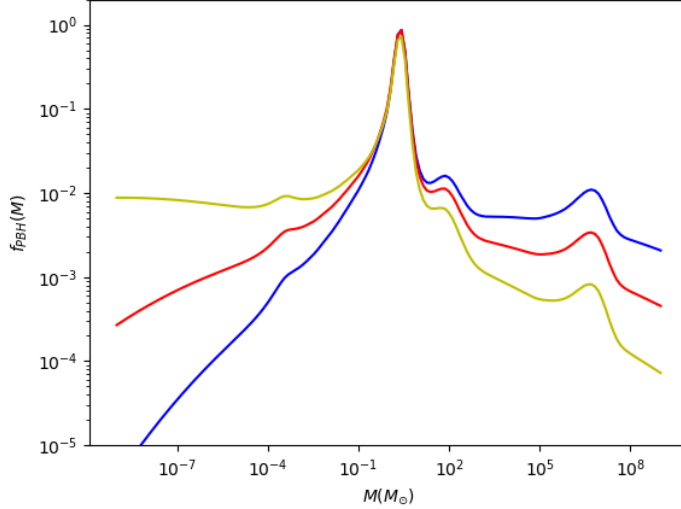
Figure 5: The mass spectrum of PBHs with spectral index $n_s = 0.95$ (blue line), $n_s = 0.96$ (red line) and $n_s = 0.97$ (yellow line).

4.3 Event likelihood

To say something about the likelihood of detecting PBH mergers, we need to first know the rate at which PBH mergers happen. To do this, we assume that PBHs comprise all of the dark matter in the Universe, which is reasonable based on Fig. 5, where the total fraction of CDM in PBHs $f_{PBH}^{tot} \approx 1$ for all three spectral indices. Then, we fill in the known cold dark matter density of the universe and multiply it with $f_{PBH}(M)$ to get the density of PBHs with a mass around M. By then specifying a volume of space we get the expected number of PBHs with a mass around M inside this volume $n_{PBH}(M)$. We then use the expression for the capture rate τ_{PBH}^{capt} of a black hole of mass m_A by a black hole of mass m_B from Ref. [7]

$$
\begin{aligned}
\tau_{PBH}^{capt} = 2\pi \ n_{PBH}(m_A) \ \bar{v} \left(\frac{85\pi}{6\sqrt{2}} \right)^{2/7} \\
\times \frac{G^2 (m_A + m_B)^{10/7} (m_A m_B)^{2/7} c^{18/7}}{c^4 v_{rel}^{18/7}},
\end{aligned}
\tag{16}
$$

where $\bar{v}$ is the average velocity of the PBHs and v_{rel} is the relative velocity of the two PBHs. From this, we can calculate the total merging rate τ_{tot}, again dependent on the volume we choose:

$$
\tau_{tot} = \tau_{PBH}^{capt} \ n_{PBH} \ \mathrm{yr}^{-1} \ \mathrm{Volume}^{-1}.
\tag{17}
$$

14

Now that we now the merger rate, we look at the detectability of an event. For this, we use the luminosity distance of the furthest detectable source R_{det} from [3]

$$R_{det} = \frac{\sqrt{5}}{24} \frac{(G\mathcal{M}c^3)^{5/6}}{\pi^{2/3}} \times \frac{1}{2.26} \left[\int_{f_{min}}^{f_{max}} df \frac{f^{-7/3}}{S_h(f)} \right]^{1/2},$$ (18)

where $\mathcal{M} = (m_1 m_2)^{3/5}/(m_1 + m_2)^{1/5}$ is the chirp mass and $S_h(f)$ is the noise power spectral density. Finally, we get the event likelihood by multiplying Eq. 17 and the cube of Eq. 18, to account for the three possible spatial axes:

$$\text{Event likelihood} = \tau_{tot} \cdot R_{det}^3.$$ (19)

5 Results

In this thesis we have converted the Mathematica notebook used in Ref. [3] into a Python notebook [15]. The notebook starts off with defining some basic cosmological constants and functions. Then, we import all the data files needed and do the first interpolations of them. This gives Fig. 4. The code proceeds to implement the functions from section 4.2, where we use the numerical results for δ_c from Ref. [12]. From this, we get the mass spectra as shown in Fig. 5. For the calculations in the remainder of the code, we use the spectrum with $n_s = 0.97$, since this is the same value for the spectral index as for the Cosmic Microwave Background. With a spectral amplitude of $A = 0.1480$, we get for the total dark matter fraction $f_{PBH}^{tot} = 0.9709$. Since this is very close to one, it justifies assuming that all of the dark matter is in PBHs, as noted before. To calculate the PBH merger rate, we first look at the number of PBHs with a mass around M in a cubic parsec:

$$n_{PBH} = \delta_{PBH}^{loc} \frac{\rho_{PBH}}{m_{PBH}} \text{ pc}^3,$$ (20)

where δ_{PBH}^{loc} is the local density contrast in PBH (taken to be equal to 10^9) and ρ_{PBH} is the

PBH density in the Universe (taken to be equal to the cold dark matter density). We us this n_{PBH} in Eq. 16, together with $\bar{v} = 2000 \; m/s$ and we take $v_{rel} = \bar{v}$. For the total merger rate, we take the volume to be one cubic gigaparsec. For the $S_h(f)$ in Eq. 18 we interpolate data from the LIGO/Virgo spectral noise densities for the O2 runs and we take $f_{min} = 10$ together with f_{max} ranging from 20 to 2000, depending on the chirp mass. Using all of this in Eq. 19, with masses ranging from $10^{-0.5}$ to $10^{2.5}$, results in the contour plot shown in Fig. 6. In this plot, you can again see peaks corresponding to the peaks of Fig. 5, but now with their
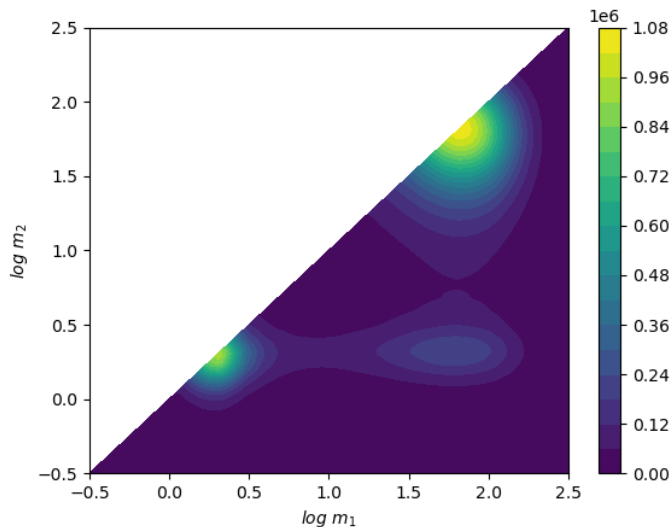

Figure 6: Contour plot of the likelihood of detecting a binary PBH merger with masses m_1 and m_2. We only consider the region where $m_1 > m_2$, which is the convention.

detectability by LIGO/Virgo in mind. This results in the peak at around $m_1, m_2 \approx 100 M_\odot$ to be the brightest and the peak at $m_1, m_2 \approx 2M_\odot$ to be fainter. Although black holes with a mass around $100 M_\odot$ lie in the upper mass gap of astrophysical black holes, they can be formed from earlier mergers of astrophysical black holes or through mass accretion. This means that we can not for certain say that they are of primordial origin even though we have a peak in the mass spectrum of PBHs there. For mergers of objects with masses of a few solar masses, we can also not for certain say they are from PBHs, since these mergers could also correspond to the coalescence of NSs with similar masses. However, it might be possible to distinguish these two kinds of events: NSs mergers yield an electromagnetic signal counterpart, whereas (primordial) black hole mergers do not. If we get a merger in this mass range close-by enough that we should be able to see the electromagnetic counterpart, we should be able to confirm

their PBH origin if we do not detect such a counterpart. The only mass range where we can for sure say that we only have a PBH merger, is for the sub-solar range. In Fig. 5 you can see a small peak at masses around $5 \times 10^{-4} M_\odot$. The problem is however, that the detectors are currently not sensitive enough to detect mergers with these masses.

6 Conclusions and discussion

In this thesis we found that the mass spectrum of a possible primordial black hole population is greatly affected by the thermal history of the early Universe; peaks in the spectrum are found whenever the number of relativistic degrees of freedom changes. From this spectrum, and by taking into account the sensitivity of the LIGO/Virgo detectors in their O2 run, we find that PBH mergers with both masses around $2M_\odot$ or with both masses around $100M_\odot$ are detectable with current laser interferometers. In obtaining our results, we have assumed that PBHs comprise all of the cold dark matter, which is a reasonable assumption based on Fig. 5. To confirm the mass function for PBHs we found, or the existence of PBHs in general, we must detect GWs that can only be explained by PBHs. As stated in the results, we should be able to detect BH mergers with masses around $2M_\odot$ or $100M_\odot$, but we can not for certain say they are of primordial origin. If we detect a lot of mergers with these masses however, more than we would expect if they do have some sort of astrophysical origin, we could argue that they are indeed from PBHs. For the $2M_\odot$ mergers we can also distinguish between NS mergers and PBH mergers by the existence of an electromagnetic counterpart signal. At the moment, there are not enough detections in these mass ranges to clearly say that PBHs exist, but with future detector runs (O3b / O4) this could change. In the future, as the sensitivity of the detectors is increased or when new detectors are built (for example Einstein telescope and LISA), it may also be possible to probe mergers in the sub-solar mass region. This region is very important for PBH searches, since this is the only region where you can exclusively have PBH mergers. Another topic for future research is simulating the waveforms coming from PBH mergers with different (chirp) masses, so that they can be used in the GW template banks. Finally, we can in the future look at the spins of the black holes in mergers to find PBHs, since PBHs are expected to have very low spins, whereas astrophysical black holes usually have quite large spins.

A   Appendix

A.1   Interpolator

Since we use quite some interpolations for our results and figures, there are bound to be some differences between the two notebooks. This is because different programming languages may have slightly different definitions and precision's when it come to interpolating. As we have seen, this is definitely the case for Mathematica and Python. For most of the interpolations, the difference is really small and therefore not significant for the numerical results. There are some instances however, where the difference is noticeable. This is the case whenever the Mathematica notebook uses the standard 'Interpolation' function. This function does a third order Hermite interpolation whereas the standard Python interpolation function 'scipy.interpolate.interp1d' uses a spline interpolation. There is a function called 'scipy.interpolate.PchipInterpolator' that uses a Piecewise Cubic Hermite Interpolating Polynomial (PCHIP), but this gives in general a bigger difference compared to the Mathematica notebook than the standard cubic 'interp1d' interpolation, as can be seen in Fig. 7 and especially in the zoomed in figures. From these figures you can clearly see that there is a big discrepancy in the lower mass end of the spectra between the two notebooks. Although this mass range does not have a peak in f_{PBH} (see Fig. 5), it is still cause for concern. Another concern is the smaller peak in percentage difference around the 10^{-1} to $10^2 M_\odot$, since this mass range has the biggest peak in f_{PBH}. Because the difference is a few percent, you can not really see the differences in the plots, but you can see it in the numerical results. Important to note here is that the mass spectra are used throughout the rest of the code, so there is a discrepancy between almost all the numerical results of the notebooks.
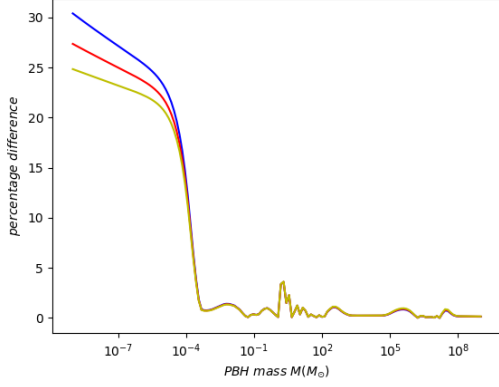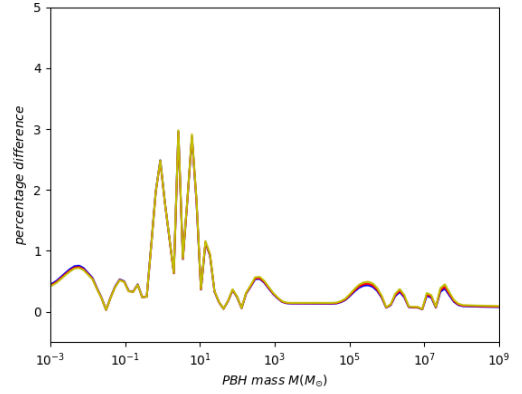
(a)
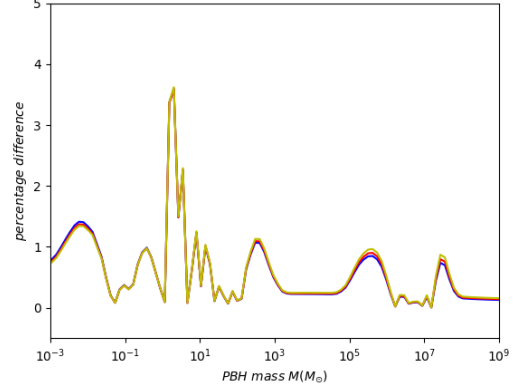
(b)
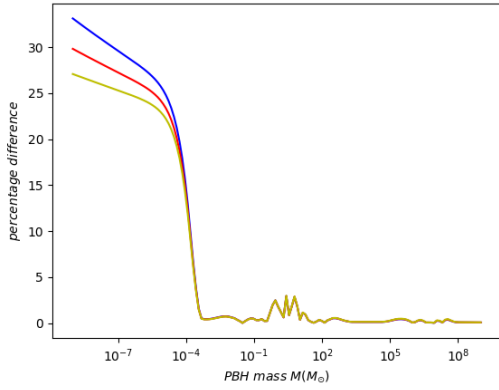
(c)

(d)

Figure 7: The percentage difference between the Mathematica notebook and the python notebook for the PBH mass spectra of the different spectral indices $n_s = 0.95$ (blue line), $n_s = 0.96$ (red line) and $n_s = 0.97$ (yellow line) using PCHIP interpolation (figures (a), (b)) and cubic interp1d interpolation (figures (c), (d)). Figures (a) and (c) are the percentage differences across the entire mass range and figures (b) and (d) are more zoomed in.

References

[1] BP Abbott, R Abbott, TD Abbott, S Abraham, Fausto Acernese, K Ackley, C Adams, Rana X Adhikari, VB Adya, C Affeldt, et al. Binary black hole population properties inferred from the first and second observing runs of advanced ligo and advanced virgo. *The Astrophysical Journal Letters*, 882(2):L24, 2019.

[2] Nabila Aghanim, Yashar Akrami, M Ashdown, J Aumont, C Baccigalupi, M Ballardini, AJ Banday, RB Barreiro, N Bartolo, S Basak, et al. Planck 2018 results-vi. cosmological parameters. *Astronomy & Astrophysics*, 641:A6, 2020.

[3] Bernard Carr, Sebastien Clesse, Juan Garcia-Bellido, and Florian Kühnel. Cosmic conundra explained by thermal history and primordial black holes. *Physics of the Dark Universe*, 31:100755, 2021.

[4] Bernard Carr and Florian Kühnel. Primordial black holes as dark matter: recent developments. *Annual Review of Nuclear and Particle Science*, 70:355–394, 2020.

[5] Bernard J Carr. The primordial black hole mass spectrum, 1975.

[6] Elisa Chisari. Lecture notes on cosmology.

[7] Sebastien Clesse and Juan García-Bellido. The clustering of massive primordial black holes as dark matter: measuring their mass distribution with advanced ligo. *Physics of the Dark Universe*, 15:142–147, 2017.

[8] LIGO Scientific Collaboration. Sources of gravitational waves. `https://www.ligo.org/science/GW-Sources.php`.

[9] Lars Husdal. On effective degrees of freedom in the early universe. *Galaxies*, 4(4):78, 2016.

[10] M Mapelli. Binary black hole mergers: formation and populations. *Front. Astron. Space Sci. 7: 38. doi: 10.3389/fspas*, 2020.

[11] Pablo Marchant, Norbert Langer, Philipp Podsiadlowski, Thomas M Tauris, and Takashi J Moriya. A new route towards merging massive black holes. *Astronomy & Astrophysics*, 588:A50, 2016.

[12] Ilia Musco and John C Miller. Primordial black hole formation in the early universe: critical behaviour and self-similarity. *Classical and Quantum Gravity*, 30(14):145009, 2013.

[13] G. Steigman. Counting relativistic degrees of freedom. `https://ned.ipac.caltech.edu/level5/March02/Steigman/Steigman1_2_1.html`.

[14] Chris van den Broeck. Lecture notes on gravitational waves.

[15] Joren Ziel. Python code and data files. `https://github.com/JorenZiel/Bachelor_Thesis`.